Direct Analysis of a Steel Railway Bridge via Monitoring System of an Instrumented Structure

Wimpie Agoeng Noegroho Aspar [a], Mulyo Harris Pradono [b], Willy Barasa [a], Suci Putri Primadiyanti [a], Leonardus Setia Budi Wibowo [b,*], Dwi Agus Purnomo [a], Emeralda I N S P J D S Pasadena [a]

[a] Research Center for Transportation Technology, National Research and Innovation Agency (BRIN), South Tangerang, Indonesia
[b] Research Center for Structural Strength Technology, National Research and Innovation Agency (BRIN), South Tangerang, Indonesia
Corresponding author: *leon004@brin.go.id

Abstract—**Railway infrastructure maintenance is essential in implementing the transportation system. Most of these railway bridges have suffered gradual deterioration over time. Predictive structural health monitoring (SHM) is required by installing instrumentation sensors on railway bridges to determine the condition of the railway bridge infrastructure at the site. This research aims to analyze and assess the existing condition of steel railway bridges to understand the load-deformation characteristics, bearing capacity, and dynamic response of the structure. This paper describes a valuable method for assessing the condition of steel railway bridges during operation. This paper presents a direct analysis of the steel railway bridge structure, with a span of 40.00 meters, a width of 4.40 meters, and a height of 6.60 meters. The steel structure railway bridge is modeled in 3D in detail, and numerical analysis is carried out using finite element analysis based on input parameters obtained from manual field measurements and instrumentation sensors. The expected result of the development of this SHM System is to know the performance of the steel railway bridge structure in real-time via the dashboard display. The results showed that the carrying capacity of the railway bridge was in a relatively safe condition. This case study may help practice engineers and researchers in future research. It can be a valuable reference for future research in developing and applying such a system to a typical case.**

Keywords— **Dynamic response; instrumentation sensors; load deformation; railway bridges; structural health monitoring.**

I. INTRODUCTION

Railway lines were built to connect separate areas with relatively dense traffic density. When railroads cross obstacles, such as valleys, rivers, highways, or seas, bridges are needed to connect them. Bridges are essential infrastructure for the rail transportation network. This bridge functions as a mode of transportation to transport natural resources in the form of coal and heavy industrial products and as a mode of public transportation for passenger and goods transportation. During their design life, railway bridges experience degradation due to natural disasters or other environmental influences such as extreme temperature changes, corrosion, and loading conditions. Frequently, these railway bridges continue to experience increasing operational demands regarding axle load and operating frequency. Due to the increased freight volumes in Indonesia, railway bridge loading conditions have been adjusted in recent decades [1]. Moreover, many of the railway bridges have experienced gradual deficiencies over time and have finally deteriorated structurally. The rehabilitation and life extension of these structures pose important maintenance and safety issues.

Researchers observed that natural and human activities might cause performance degradation of railway bridges. The combination of these effects can deteriorate the structure of railway bridges. If this damage is not detected at a reasonable early stage, it can lead to a catastrophic bridge failure. Therefore, the bridge's infrastructure must be monitored for signs of failure [2]. Experts usually establish damage criterion techniques according to the analysis of vibration data to help field observation procedures. Many researchers have established damage detection strategies and assessments for various railway bridge structures over the past decades [3]–[11]. The results of this study indicate the development of various Structural Health Monitoring (SHM) techniques according to different parametric damage detection techniques to improve the ability to assess the condition of existing railway bridges.

To guarantee the validity of data recording via SHM, careful observation is needed regarding the position, speed, and load of trains using sensors installed in critical locations on the railway bridge. Furthermore, the installed instrument's data is utilized to directly analyze the railway bridge structure. In general, previous inspections of bridge conditions were mostly done visually and non-destructively testing, which may not be very accurate in obtaining data depending on the level of expertise of researchers in the field. In general, inspecting the previous condition of bridges is mostly done visually and non-destructively testing, which may not be very accurate in obtaining data depending on the level of expertise of researchers in the field. This practice is often disrupted if continuous monitoring of bridges is carried out because the operation of railway bridges cannot be stopped [12]–[22]. Therefore, a comprehensive SHM is needed without disrupting the operation of trains passing the railway bridge. The data obtained from the measuring sensor using the SHM technique can be directly used to analyze the health condition of the railway bridge structure. Many researchers make observations to get real data by applying low-cost instrumentations installed on the rail bridge to determine vertical and transverse deformation [23]–[27]. This study suggests that transverse deformation can provide an assessment of the condition of a railway bridge. The initial implementation of the SHM was applied to analyze the strength of the profiles attached to the workforce on the railway bridge. Vertical deflection, capacity ratio, and natural frequency of railway bridges during operation can be observed directly [28].

To maintain reasonably good construction performance of the railway bridges during post-construction, it is necessary to understand a railway bridge's significant parameters. A loading combination is a significant parameter that should be observed. The structural performance of bridges damaged by moving loads or deficient existing bridges is becoming increasingly crucial for evaluation and inspection. To deal with this condition, it is necessary to have a monitoring system that can automatically and directly detect the behavior of structural railway bridges. The development of damage detection techniques can be applied to monitor whether the structure's service life has exceeded the design limit. When long-term monitoring of bridges is required, instrumentations are usually installed to determine the dynamic characteristics of the railway bridge [29]–[32]. A common practice of the railway bridge detection technique for its structure under moving vehicle loads was analyzed numerically and verified experimentally [33]–[37]. Field measurements using instrumentation sensors are necessary for actual investigation. The sensors that can monitor the vibration due to loading on the bridge are accelerometers. An accelerometer is a sensor that can measure acceleration and detect and measure vibrations [38], [39].

This paper describes a valuable method for assessing the condition of steel rail bridges during operation. This paper analyses and assesses the condition of the existing steel rail bridge structure. The expected result of developing this SHMS is understanding the real-time performance of the steel railway bridge structure through the dashboard display. SHMS is scheduled as an early warning system and can assist the decision-makers in taking the appropriate measures to maintain the reasonable performance of railway bridges.

II. MATERIALS AND METHOD

A. Overview of Existing Railway Bridge Case Study

The object of the research study is a steel railway bridge structure located in Rangkasbitung, Banten Province, Indonesia. The study analyzes and assesses the current steel structure railway bridge condition. The steel railway bridge is a three supported spans of steel structure with 40.0 m in span length, 40.0 m of middle span, and 25 m of the other span. However, only the first span was considered and analyzed in this study. It is a one-lane steel structure railway bridge and seats on wooden sleepers. The steel railway bridge has a vertical height of 6.60 m with a Warren configuration for the longest span. The railway bridge is 4.40 m wide for all spans, with side bracing and no top bracing for the shortest span. Fig. 1 illustrates the longitudinal perspective of the steel railway bridge with the cross-sectional view and its surrounding environment.

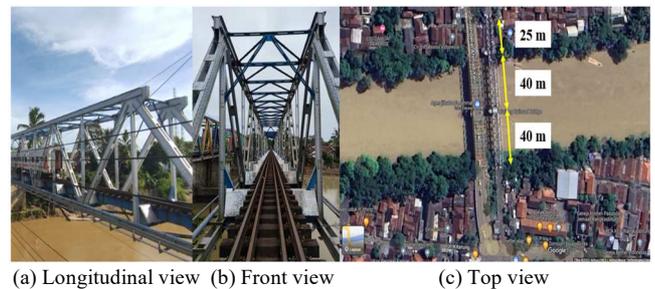(a) Longitudinal view (b) Front view   (c) Top view
Fig. 1 The Overview of Existing Railroad Bridge

The steel frame bridge used is the WF and angled profiles, which are known based on the available shop drawings and clarification results of the direct inspection in the field. The material properties of custom steel girder profiles for numerical study are the steel yield stress of 210 MPa, and the maximum tensile stress of 340 MPa, respectively. Steel type girder utilizes BJ 34 (RSNI T-03-2005 with an elasticity modulus of 200.000 MPa, steel density of 76.189 kN/m^3, and Poisson's ratio of 0.3, respectively.

The structural plan of the steel railway bridge structure is shown in Fig. 2. The dimension of the frame profiles is known based on as-built drawings and additional direct inspection in the field for rechecking. The existing state of the location and the value of actions should be identified by the in-situ measurement and compared to available bridge documentation. A numerical analysis of the railway bridge is executed to simulate and understand the deformation, stress distribution, and natural frequency characteristics. These three parameters are the basis for the instrumentation placements of the sensors and for selecting the sensor types to be installed.

B. Theoretical Background

Direct numerical analysis of a structure gives a dynamic prediction of the structural characteristics of the structures. The dynamic responses of a structure involve accelerations, velocities, and displacements. The dynamic equilibrium equation regarding the structure's response to the ground

motion is governed by the equation of motion [40] and is given as in equation (1):

$$M\ddot{u}(t) + C\dot{u}(t) + Ku(t) = F(t) \qquad (1)$$

in which M, C, and K represent diagonal mass, proportional damping, and stiffness matrices of the system, respectively. The relative deformation, velocities, and accelerations concerning the dynamic motion are represented by u, $\dot{u}$, and $\ddot{u}$, respectively. Equation (1) is a linear dynamic response of a structure with N degrees of freedom. F. represents the external forcing of the system If the free response is considered, Equation (1) can be simplified to find a response for the 1st degree of freedoms and an N degree of freedoms, then equation (1) can be written as in equation (2)

$$M\ddot{u}(t) + C\dot{u}(t) + Ku(t) = m_x\ddot{u}_{gx}(t) + m_y\ddot{u}_{gy}(t) + m_z\ddot{u}_{gz}(t) \quad (2)$$

where m_x, m_y, and m_z are the unit acceleration loads. The components of uniform dynamic acceleration are represented by $\ddot{u}_{gx}$, $\ddot{u}_{gy}$, and $\ddot{u}_{gz}$, respectively.

(a) Top view of the Structural Plan
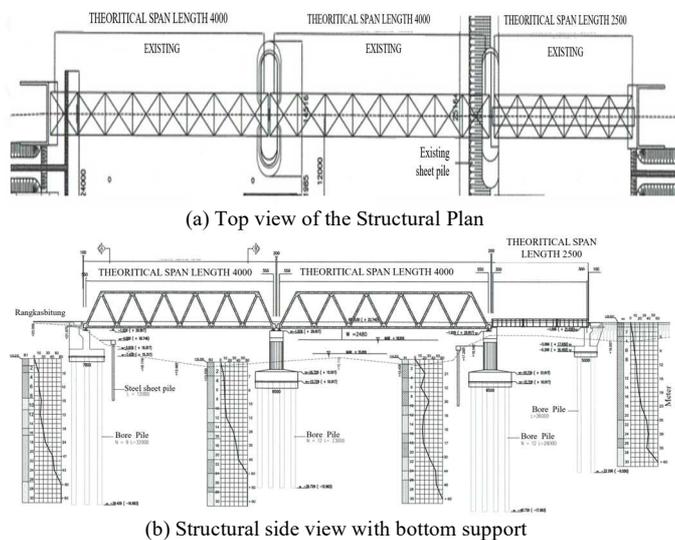

(b) Structural side view with bottom support

Fig. 2 Structural plan of the Steel Railway Bridge Structure

Dynamic response in every direction can be a digitized response-spectrum curve of pseudo-spectral acceleration response versus a period of the structure [41]. To understand the behavior of the structure, it is helpful to apply model analysis. Modal analysis is utilized to find the vibration modes of a structure. The modal time history and response spectrum for load cases can be analyzed using modal superposition. The method of nonlinear time-history analysis was developed [42]. The technique is significantly useful, especially for structural systems with predefined nonlinear elements. It is widely recognized as a fast nonlinear analysis and is commonly applied for SAP2000 numerical software [43].

C. Railway Bridge Structural Modelling

This railway bridge is passed by coal transport trains, passenger trains, and freight trains for daily transporting heavy industrial products. The railroad lines are relatively hectic, and the fairly high freight volumes with increased loading caused the gradual degradation of the steel railway bridges over time. In this study, the steel structure railway bridge was 3D modeled in detail, and the numerical analysis was performed using finite element analysis. Finite element

analysis was done using SAP2000® Ver software 6.113 [41]. Subsequently, the railway bridge was modeled and analyzed numerically.

Furthermore, the steel railway bridge in a three-dimensional (3D) model was established using the SAP2000 software package, according to field observation data, material properties, and relevant shop drawings. The structural model is beam elements reflecting the structural frame members, in which some links connect the abutment. The material properties of the steel bridge structure were adopted as mentioned in the specification. To avoid discrepancies in data reading due to sensor data anomaly, it is suggested that before performing the loading on the railway bridge, all installed instrumentations were calibrated to have functional valid data collection [44]. The schematic instrumentation layout of these railway bridge sensors is shown in Fig. 3. In modeling, ways are carried out to make the model as straightforward as possible while still simulating the behavior of the actual bridge structure under different loading conditions. This model shows that the developed railway bridge model is valid enough to assess the structural performance effectively under simulated loading conditions.
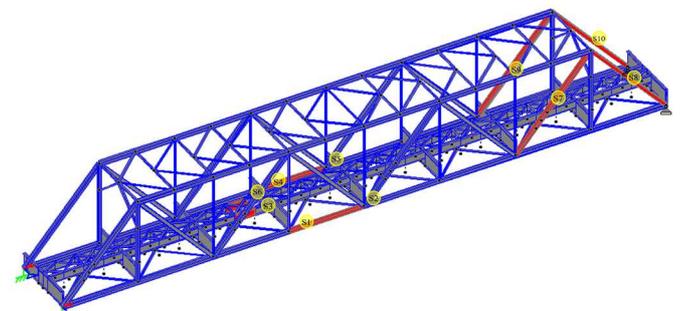
(a) Illustration of Strain Gages Installation Location
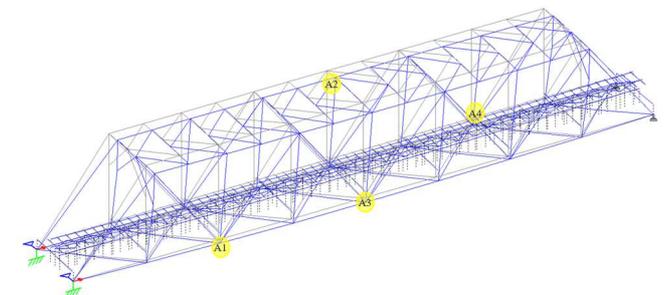
(b) Illustration of Accelerometer Placement
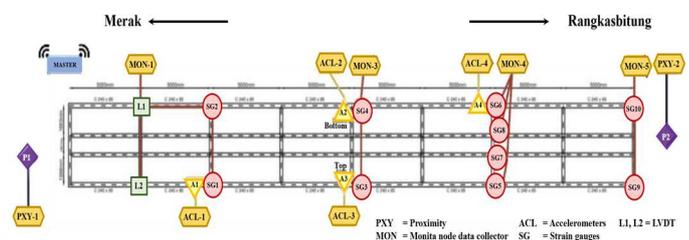
(c) Schematic View of Instrumentation Placement

Fig. 3 Schematic Location of the Instrumentation Placement on the Railway Bridge

The abutment end of the railway bridge is assumed to be a hinge, while rollers support the other end during finite element modeling analysis. Some assumptions were made for modeling and analyzing the steel railway bridge. It was

assumed the supports have no frictional resistance to have translational restraint without inducing rotational restraint. As previously described, the steel railway bridge was modeled and analyzed using the SAP2000 software [41]. The schematic 3-D finite element model of the bridge structure is illustrated in Fig. 4.

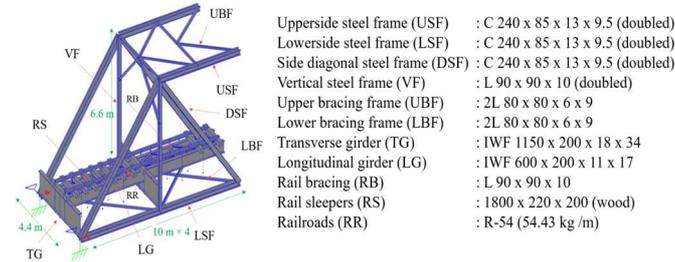| Upperside steel frame (USF) | : C 240 x 85 x 13 x 9.5 (doubled) |
Lowerside steel frame (LSF)	: C 240 x 85 x 13 x 9.5 (doubled)
Side diagonal steel frame (DSF)	: C 240 x 85 x 13 x 9.5 (doubled)
Vertical steel frame (VF)	: L 90 x 90 x 10 (doubled)
Upper bracing frame (UBF)	: 2L 80 x 80 x 6 x 9
Lower bracing frame (LBF)	: 2L 80 x 80 x 6 x 9
Transverse girder (TG)	: IWF 1150 x 200 x 18 x 34
Longitudinal girder (LG)	: IWF 600 x 200 x 11 x 17
Rail bracing (RB)	: L 90 x 90 x 10
Rail sleepers (RS)	: 1800 x 220 x 200 (wood)
Railroads (RR)	: R-54 (54.43 kg /m)

Fig. 4 Schematic 3D Finite Element Model of the Steel Structure Railway Bridge

The bridge components consist of upper-side steel frame (USF), lower-side steel frame (LSF), diagonal steel frame (DSF), vertical steel frame (VSF), upper bracing frame (UBF), lower bracing frame (LBF), transverse girder (TG), longitudinal girder (LG), rail bracing (RB), rail sleepers (RS), and railroads (RR). The dimensions are from direct measurements of the bridge components. Based on these dimensions, a finite element model was developed. The rail sleepers and railroads were represented as an additional mass to the longitudinal girders since their stiffness was minor compared to the girders. The longitudinal axis of the bridge is named X direction, the lateral axis is Y direction, and the vertical axis is Z direction.

The numerical modeling of the railway bridge structure was modeled using two loading schemes on the bridge, namely the moving load scheme (ML) and the static load scheme (SL). In addition, the validity of actual railway bridge frames and their cross sections must also be considered. The load-bearing capacity must be complied with according to a standard way so that the structure has earthquake resistance [45]. The railway bridge was modeled with an axle load of 168 tons (1,500 kN). The numerical simulation results show considerable differences in deflection and stress due to the moving load and static load schemes.

D. Related Literature Study

Railway bridges play a significant role in a railroad transportation network. Railway bridges must be maintained to guarantee the safe operation and the existence of the railway performance network. There has been an increase in the freight demand for goods in the western part of the Java region, which must be served by rail transport. Therefore, railroad infrastructure should be maintained, especially railway bridges in the region. Railway bridge maintenance has a significant influence on the importance of the safety and availability of the rail network [46].

The establishment of railway bridge inspection measurement has been performed in many countries. The development techniques have been combined by integrating the management systems of the bridges [47]. The railway bridge inspection procedures and monitoring systems are incorporated into that system. However, establishing the railway bridge monitoring system is always dependent on the

geographic and socioeconomic conditions of the country [48]. It is necessary to regularly conduct railway bridge monitoring in geographical areas prone to natural disasters. This monitoring system is an early warning in determining damage detection of a railway bridge structure.

The service life of a railway bridge structure can be assessed beyond the basic service life of the design; therefore, a railway bridge damage detection technique is needed and needs to be developed and implemented [49], [50]. The damage detection technique in civil engineering is commonly related to structural health monitoring. The development of a damage identification framework based on the acceleration response of a railway bridge was established [51]. The damage detection technique applies the operational vibration response of a steel girder railway bridge. The analysis of acceleration and strain responses provides information regarding damage features of the steel framework of railway bridges during operation [52]. Both acceleration and strain responses were calculated based on data recorded from instrumented truss elements of the railway bridge. Numerical simulation was applied to validate the final detection.

Implementing an instrumented vehicle can indirectly perform The structural monitoring system [53]. The vehicle was instrumented with accelerometer sensors installed on its axle. The alternative technique uses the interaction of vertical trajectories at critical points on the approach of a railway bridge and the lateral misalignment associated with the bridge being placed at a sharp bend [54]. The dynamic interaction between the wheels and the rails is increasing due to the accelerated speed of the train and the heavy additional axle loads, especially in the vertical direction [55]. Therefore, it is necessary to analyze and evaluate the railway bridge's condition directly via a monitoring system of instrumented structure to satisfy the service requirement.

III. RESULTS AND DISCUSSION

A. Finite Element Modeling of the Railway Bridge

This study's developed steel railway bridge structure model is a 40,00-m-long single-span deck-type steel plate girder bridge, as illustrated in Fig. 5. The railway bridge consists of two main girders. The deck rests on nine girders equidistant from each other, with two on abutment supports. Rail bridge supports are modeled as hinges fixed to translation but free to rotate.

For railway bridges, the loads are categorized into three loading types: the girder's own weight, additional dead loads, and live loads. For the additional dead load analyzed, loading combinations of the train, including bearings, were estimated according to PM 60/2012 [56] and on a train set of CC-206 locomotives with coaches. This CC-206 is a standard locomotive on this rail track. The live load acting on the structure of the railway bridge is the load originating from the railroad circuit, the amount of which is determined based on the 1921 Load Plan (RM 1921). The loadings applied in railway planning complies with the PM 60/2012 standard, and it is explained as described in Fig. 6. The uniform loading is 8.75 tons (78 kN) per meter. The RM 1921 assumes two sets of locomotives with tenders. The length of one set is 19.2 meters. Therefore, for two train sets, the length will reach that of the bridge (40 m). The application of this load to the railway bridge is shown in Fig. 7.
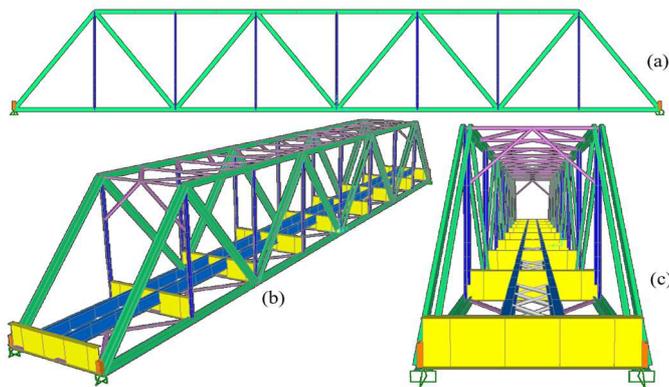
Fig. 5 FEM Model of the Train Bridge; (a) Side view, (b) 3D Perspective View, and (c) Front View
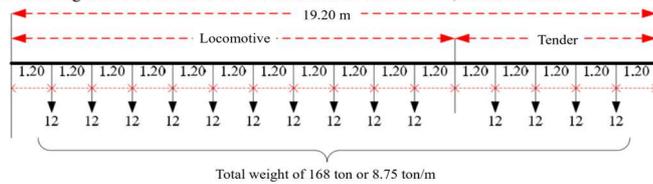
(DESIGN LOAD 1921)

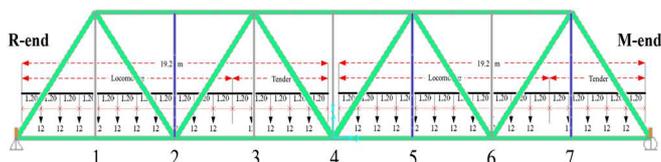Fig. 6 Loading Scheme of Load Plan 1921 (RM21) [56]

Fig. 7 Locations 1 – 7 and RM 1921 Load at the Model

Finite element modeling (FEM) of the railway bridge was carried out by applying locomotives and passenger coaches under the loading and unloading phases. The average traction force of the locomotives is about 248.00 kN. The locomotives and passenger coaches were positioned symmetrically and asymmetrically in different spans to obtain maximum internal forces and deformations of the leading carrying structural elements. The train set of CC-206 locomotive with passenger coaches is pictured in Fig. 8 [57], [58]. It contains a locomotive with a length of 15.849 meters and a weight of 90 tons (800.00 kN). Its maximum speed is 120 km per hour—the locomotive tracts passenger coaches, which are usually eight coaches. One coach's length is 20.92 meters, and its weight is 60 tons (535.00 kN).

### B. Assessment of Loading and Deformation Characteristics

To reproduce the structural response accurately, precisely measured loading actions during the trajectory of each train are introduced as input in the numerical model. Using field measurements of the instrumentation sensor array, which is mounted on the railway bridge frame, the obtained train speed, axle configuration and type of train are identified [59]. The loading characteristics are then carried out for the dead load and the four train positions, which usually pass through the rail bridge.

When entering the bridge, the position of the train set can be divided into four positions. The position I when the locomotive enters the railway bridge. Position II when the locomotive and passenger train cars cross the railway bridge.

Position III, when the locomotive reaches the end of the railway bridge, one full passenger car and half of the passenger cars cross over the railroad bridge. Position IV when two passenger trains cross over the railway bridge. Their typical speed on the railway bridge is 120 km/h. The average axle load of this train is presented in Fig. 9.
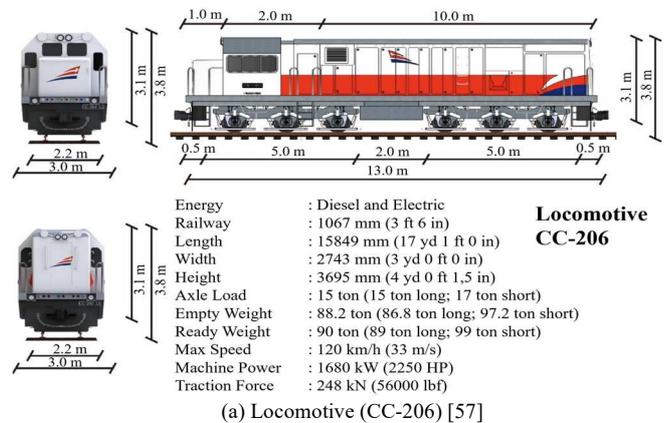
(a) Locomotive (CC-206) [57]
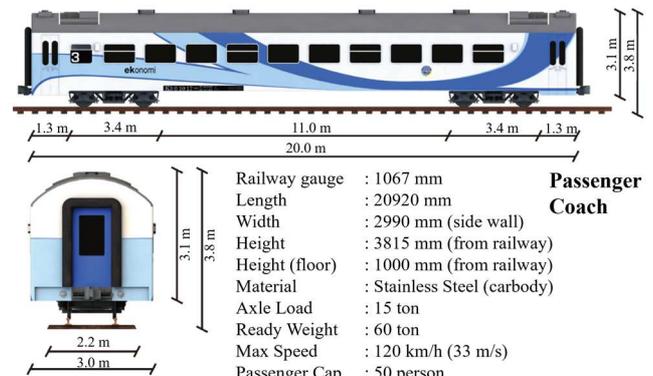
(b) Passenger Coaches [58]

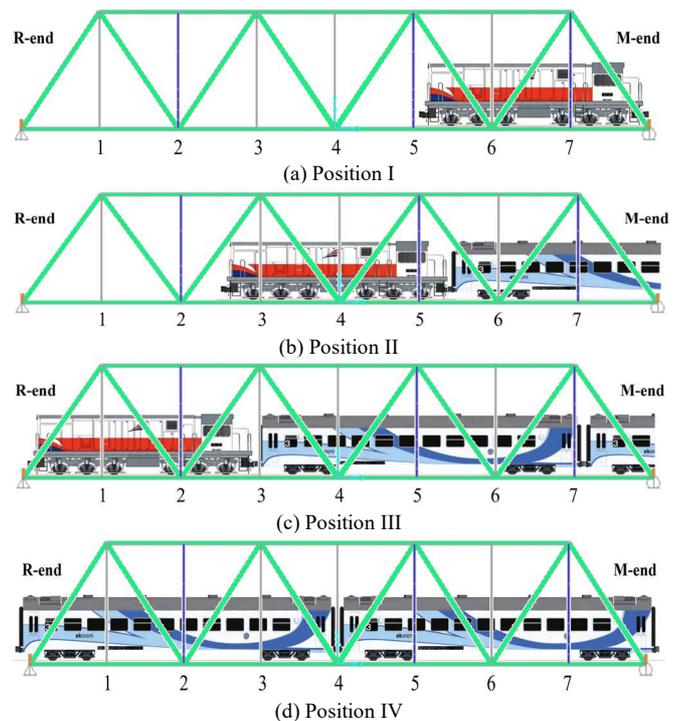Fig. 8 Loading from Train (Locomotive and Passenger Coaches)

(a) Position I

(b) Position II

(c) Position III

(d) Position IV

Fig. 9 Loading Configuration from the Trian Load under Positions I-IV

The dynamic numerical simulation carried out in this work aims to reproduce the structural quantities measured at the exact location from the real sensors installed at the site when the train crosses over the railway bridge. The sequence of train positions produces different kinds of loads for the railway bridge. This can be assumed to be the load of a moving train at the railway bridge. The response results can directly be compared to the sensors' reading at the railway bridge. The responses of interest are deformations, stresses, and accelerations at some points of the railway bridge.

The deformation numerically was carried out for the railway bridge under the proposed loading conditions. The railway bridge deformation took place in the three directions, X, Y, and Z axes, respectively. Under the dead load and the load train passing the railway bridge, the deformation occurring at every railway bridge can be observed. The magnitude of deformation that occurs is tabulated as shown in Table 1. Fig. 10 shows the deformation locations of 1 until 7 in the model due to the loads on the railway bridge.

TABLE I
DEFORMATION DUE TO APPLIED LOAD

| Deformation (mm)	Location – Dead Load						
	1	2	3	4	5	6	7
X	0.22	0.44	0.92	1.40	1.88	2.35	2.58
Y	0.04	0.06	0.09	0.08	0.09	0.06	0.04
Z	-3.24	-5.53	-7.23	-7.65	-7.23	-5.53	-3.24
	Location – RM 1921 Load						
	1	2	3	4	5	6	7
X	1.47	2.94	6.10	9.26	12.43	15.57	17.05
Y	0.29	0.40	0.63	0.56	0.63	0.40	0.29
Z	-22.16	-36.62	-48.35	-50.58	-48.35	-36.62	-22.16
	Location – Train Load Position I						
	1	2	3	4	5	6	7
X	0.15	0.29	0.74	1.20	1.97	2.75	3.29
Y	0.03	0.05	0.09	0.11	0.16	0.11	0.11
Z	-3.06	-5.88	-8.17	-9.78	-10.86	-9.26	-6.79
	Location – Train Load Position II						
	1	2	3	4	5	6	7
X	0.67	1.34	3.10	4.85	6.62	8.38	9.12
Y	0.13	0.21	0.35	0.31	0.35	0.22	0.15
Z	-10.55	-19.72	-26.77	27.96	-26.84	-19.89	-11.36
	Location – Train Load Position III						
	1	2	3	4	5	6	7
X	0.75	1.50	2.92	4.33	5.59	6.84	7.40
Y	0.15	0.19	0.28	0.24	0.25	0.16	0.11
Z	-10.61	-16.55	-21.18	21.37	-19.84	-14.87	-8.75
	Location – Train Load Position IV						
	1	2	3	4	5	6	7
X	0.48	0.96	1.99	3.02	4.05	5.08	5.57
Y	0.09	0.13	0.21	0.18	0.21	0.13	0.09
Z	-7.23	-11.96	-15.79	16.51	-15.79	-11.96	-7.23
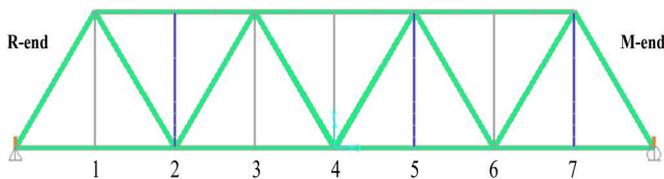
Fig. 10 Locations 1 - 7 of the Model

These figures in Table 1 show that the maximum deformation is at the midspan of the railway bridge, measuring -7.65 mm in the Z direction. The deformation caused by the RM 1921 Load is shown in Fig. 11. The maximum deformation due to this load is -50.58 mm at the midspan in the Z direction. A direct comparison of deformation by dead load and RM 1921 load is illustrated in Fig. 11. The deformation resulting from the dead load is much smaller (15%) than that due to RM 1921 load. The RM 1921 load is used for designing railway bridges in Indonesia [56].
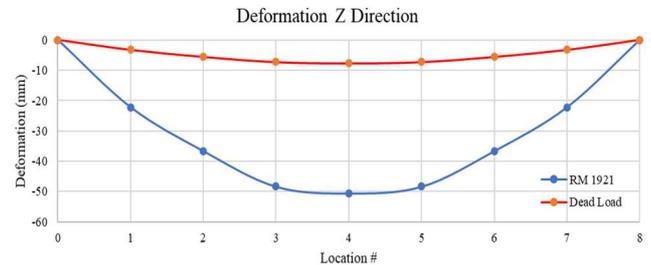

Fig. 11 Deformation of the Model in Z direction due to Dead Load and RM 1921 Load

The deformation characteristics can be observed when the train crosses the railway bridge. The deformation due to a set of the train at Position I is configured as in Table 1 just described. The maximum displacement is at Location 5 (not at the midspan), measuring -10.86 mm in the Z direction. A negative value implies the deformation is in the downward direction. Position II shows a maximum deformation of -27.96 mm at Point 4 (midspan). Position III gives a maximum deformation of -21.37 mm at Location 4. Finally, Position IV indicates a maximum deformation of -16.51 mm at Location 4.

It can be seen when the train enters the railway bridge. The largest maximum deformation occurs when the locomotive is in the middle of the span of the railway bridge, namely Position II for the Z-direction. The deformation in the Z-direction in the middle of the railway bridge span reaches 27.96 mm. Z-direction deformation resulting from numerical simulations for Positions I-IV of this study is illustrated in Fig. 12. From Fig. 12, it is clear that the most considerable Z-direction deformation occurs when the locomotive is in the middle of the railway bridge span (Position II). According to PM 60 2012 [56], a steel frame bridge's maximum permissible vertical deformation is 1/1,000 of its span. In this study, the span of the railway bridge is 40.00 meters, so the maximum allowable deformation is 40.00 mm.
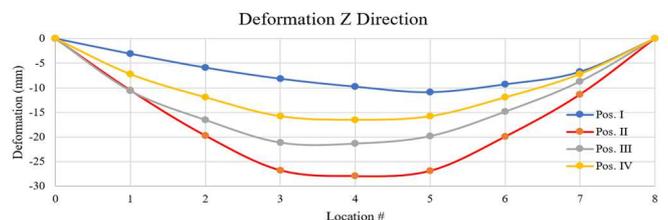

Fig. 12 Z Direction of Deformation due to Train Loads in the Model (Positions I – IV)

Compared to the numerical simulations, field measurements of the LVDT (linearly variable deformation transducer) show the same trend for both. Initially, the deformation sensor (LVDT) would be placed in the middle of the span of the railway bridge. However, the LVDT sensor was placed 5.00 meters from the Rangkasbitung (R) end due to technical considerations. Since the LVDT sensor will be located at Location 1 (or 7, depending on the direction of the

train), it is advantageous to plot deformations at Locations 1 and 7 as the train moves from right to left (*M to R*) or left to right (*R to M*), where *M* is Merak train station, and *R* is Rangkasbitung train station. Railway bridge deformation from LVDT measurements in the field is shown in Fig.13.
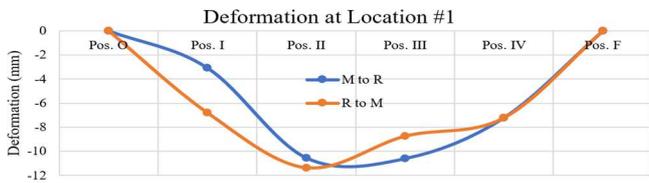

Fig. 13 Deformation at Location 1 due to Train Moving at Directions "M to R" and "R to M"

C. Working Forces and Carrying Capacity of the Railway Bridge Frame

In this research, ten strain gages are installed at the railway bridge for monitoring purposes. The ones presented in Fig. 14 are strain gages SG01 up to SG06. The SG01 and the SG02 are installed at a diagonal side frame (DSF type) near the Rangkasbitung end (*R* end), whereas the SG05 and the SG06 are installed at a diagonal frame (DSF type) near the Merak end (*M* end). The SG03 and the SG04 are installed at the lower side frame (LSF type) at the midspan of the railway bridge. The DSF and LSF types are similar in dimensions. They are C steel frames with 240 x 85 x 13 x 9.5 dimensions. These C frames are combined back-to-back with a distance, as shown in Fig. 15.
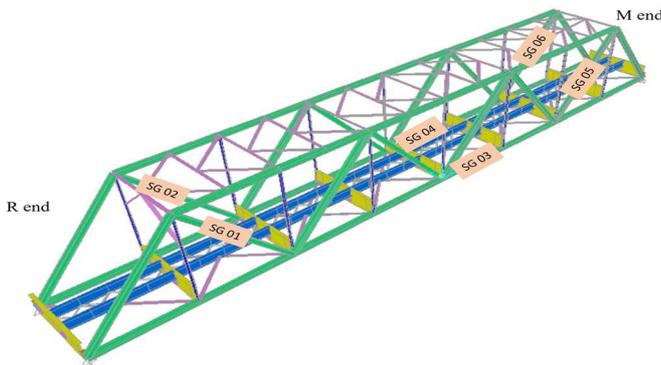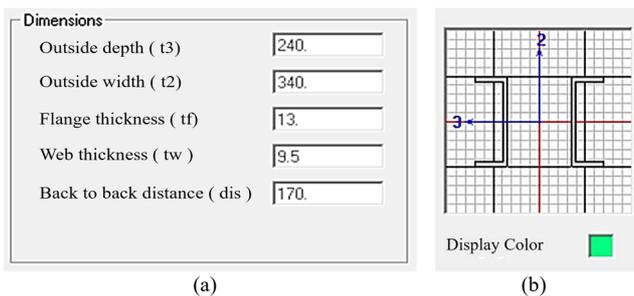

Fig. 14 Locations of Strain Gauges at the Railway Bridge

Fig. 15 DSF and LSF Types

Where (a) is dimensions in mm and (b) is a back-to-back combination of C-frame. All strain gauges installed on railroad bridges record the strain of the trusses of the railway bridge when the train passes over it. Fig. 16 illustrates the axial forces and moments generated by the train passing over the railway bridge under the Position II train loading. Fig. 16(a) shows the maximum axial forces at the upper-side steel

frame. Since the points of interest are at SG- 01, 02, 03, 04, 05, and 06, the axial forces at those points are plotted. The red color indicates that the trusses are subjected to a compression force. In contrast, the yellow indicates that the truss members are experiencing tension. The axial forces resulting from the train loading are shown in Table 2. It is observed that the axial troops at the location of SG 03 (and 04) are the largest.
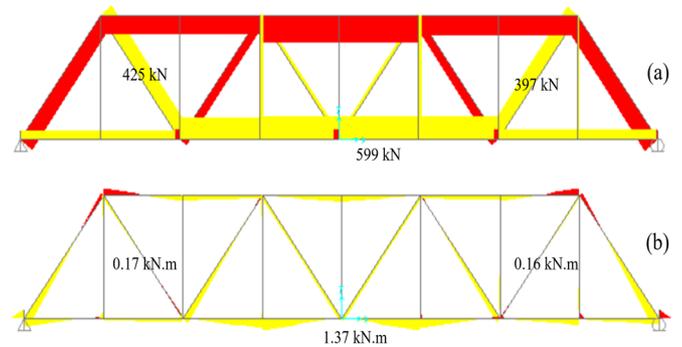

Fig 16 Distribution of (a) Axial Forces and (b) Moments at the Railway Bridge due to Train Loading at Position II

TABLE II
AXIAL FORCE AT THE LOCATION OF SG01, SG 03, AND SG05

Location	Position I (kN)	Position II (kN)	Position III (kN)	Position IV (kN)
SG01	97	425	309	223
SG03	262	599	426	350
SG05	172	397	272	223

It can be seen from Fig. 16(b) that the moments at points of interest are relatively small, so the stresses calculated from axial forces would be representative. The red indicates that the truss has a negative moment (counterclockwise). In contrast, the yellow indicates that the truss is experiencing a joyous moment (clockwise). The stresses resulting from the axial force are shown in Table 3. Fig. 17 illustrates the plots of stresses as functions of the train's positions. Train Position II indicates the most significant stresses at all SG locations. The stress ratios at SG01, SG03, and SG05 are shown in Table 4. The stress ratios are still below the elastic limit. In summary, this indicates that the railway bridge's carrying capacity is relatively safe. The ratios were calculated based on the steel yield strength, which is 210.00 MPa.

TABLE III
STRESSES AT THE LOCATION OF SG01, SG 03, AND SG05 DUE TO AXIAL FORCES

Location	Position I (MPa)	Position II (MPa)	Position III (MPa)	Position IV (MPa)
SG01	11	50	36	26
SG03	31	71	50	41
SG05	20	47	32	26

D. Dynamic Analysis of Steel Railway Bridge

Mode shapes and frequencies of the railway bridge model with no trains crossing the railway bridge are described in Fig. 18 and Table 5. Mode 1, as seen in Fig. 18(a), is in the *Y* direction with a natural period of 0.455 seconds or a frequency of 2.20 Hz. Mode 2, as illustrated in Fig. 18(b), represents *the Y direction* with a natural period of 0.196 seconds or frequency of 5.10 Hz. Mode 3, as figured in Fig. 18(c), is in the *Z* direction with a natural period of 0.171 seconds or a

frequency of 5.85 Hz. Mode 4, as pictured in Fig. 18(d), shows rotation about the *Z* axis with a natural period of 0.133 seconds or a frequency of 7.52 Hz. Finally, Mode 5, as illustrated in Fig. 18(e), describes mode shape in *X* direction with a natural period of 0.127 seconds or frequency of 7.87 Hz. The mode shape that will be excited by a passing train would be Mode 3 because of its vertical movement.
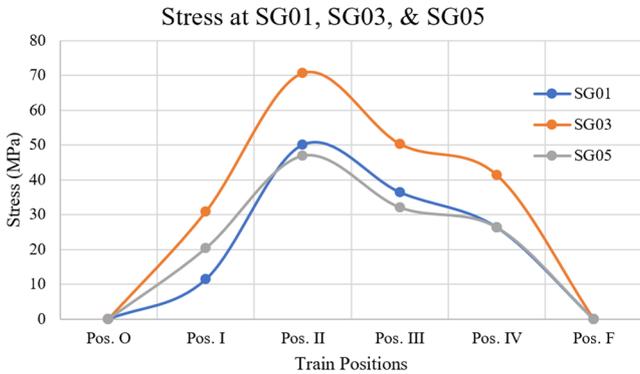
Stress at SG01, SG03, & SG05

Fig. 17 Stresses at SG01, SG03, and SG05 due to Train Loads at Positions I – IV

TABLE IV
STRESS RATIOS AT THE LOCATION OF SG01, SG 03, AND SG05

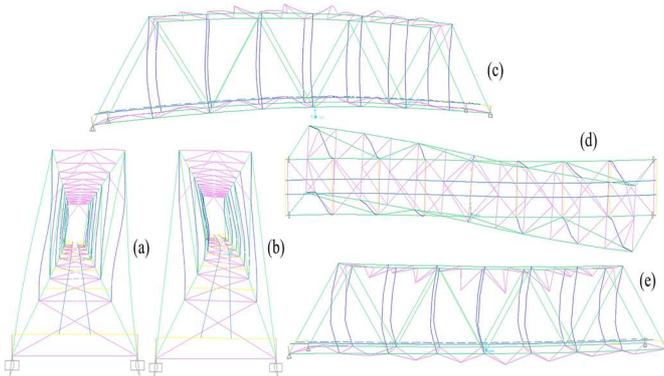| Location	Position I	Position II	Position III	Position IV
SG01	5%	24%	17%	13%
SG03	15%	34%	24%	20%
SG05	10%	22%	15%	13%

Fig. 18 Mode Shapes of the Bridge: (a) Mode 1, (b) Mode 2, (c) Mode 3, (d) Mode 4, and (e) Mode 5

TABLE V
MODE SHAPE, PERIODS, AND FREQUENCIES (WITHOUT TRAIN)

Modes	Periods (second)	Frequencies (Hz)	Directions
1	0.455	2.20	Lateral (*Y* direction)
2	0.196	5.10	Lateral (*Y* direction)
3	0.171	5.85	Vertical (*Z* direction)
4	0.133	7.52	Rotation about the *Z-axis*
5	0.127	7.87	Longitudinal (*X* direction)

The mode shape and natural frequency calculated here are in the condition that the railway bridge is not crossed by trains. A passing train may affect the railway bridge's mode shapes and natural frequencies. The train's mass may influence the railway bridge's mode shape. Since the passing time of coaches is longer than that of a locomotive, it is interesting to analyze the mode shapes and frequencies of the

railway bridge with additional mass from a row of coaches as in Position IV of Fig. 9(d).

The numerical calculation results are presented in Fig. 19 and Table 6. Mode 1, as illustrated in Fig. 19(a), is in the *Y* direction with a natural period of 0.491 seconds or a frequency of 2.04 Hz. Mode 2, as shown in Fig. 19(b), is in the *Y* direction with a natural period of 0.363 seconds or a frequency of 2.75 Hz. Mode 3, as pictured in Fig. 19(c), is in the *Z* direction with a natural period of 0.336 seconds or a frequency of 2.98 Hz. Mode 4, as seen in Fig. 19(d), is in the *Z* direction with a natural period of 0.267 seconds or a frequency of 3.75 Hz. Finally, Mode 5, as seen in Fig. 19(e), represents rotation about the *Z* axis with a natural period of 0.178 seconds or a frequency of 5.62 Hz. The mode shape that will be excited by a passing train is expected to be Modes 3 or 4, as the movements are vertical.
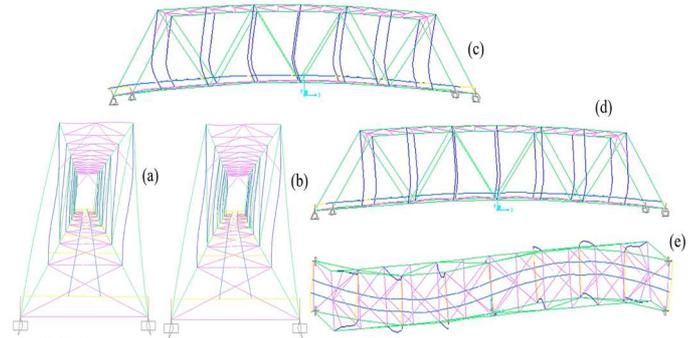

Fig 19 Mode Shapes of The Bridge with Coaches on the Railway Bridge

TABLE VI
MODE SHAPE, PERIODS, AND FREQUENCIES (WITH COACHES OF A TRAIN)

Modes	Periods (second)	Frequencies (Hz)	Directions
1	0.491	2.04	Lateral (*Y* direction)
2	0.363	2.75	Lateral (*Y* direction)
3	0.336	2.98	Vertical (*Z* direction)
4	0.267	3.75	Vertical (*Z* direction)
5	0.178	5.62	Rotation about the *Z-axis*

Another interesting phenomenon is the points where the accelerometer is attached to the railway bridge. They are accelerometers: ACCL 1, ACCL 2, ACCL 3, and ACCL 4. The locations on the railway are illustrated in Fig. 20. All were attached to the bottom side of the railway bridge. Accelerometers are installed to measure vibration from trains moving on the railway bridge. For the model to be vibrated, the vibration source is a seismic ground excitation.
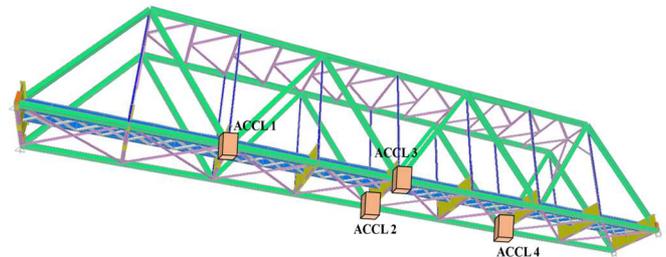

Fig. 20 Locations of Accelerometers: ACCL 1 – ACCL 4 at the Railway Bridge

The 1940 El Centro earthquake [60]–[62] ground acceleration in the N-S direction is utilized as the input ground acceleration to the railway bridge. The acceleration time

history is illustrated in Fig. 21(a). The peak ground acceleration of this earthquake is 123 gal (cm/s^2). This earthquake input is used because its frequency contents are entirely distributed, as illustrated in Fig. 21(b). Fig. 21(c) presents the acceleration response spectrum for the 5% damping ratio. Response spectrum is widely applied for understanding the structure's dynamic response given the structure's natural period. Based on the spectrum, the structural acceleration response would be amplified for structures with natural periods between 0.05 and 1.0 seconds. For the first mode shape of the railway bridge, which has 0.45 seconds of the natural period, the response would be amplified to 319 gals. However, since the railway bridge is a multi-degree-of-freedom structure, its higher modes would also affect the results, as will be discussed in the following paragraphs.

(a) Ground Acceleration

(b) FFT (Fast Fourier Transform) Single-sided Amplitude Spectrum
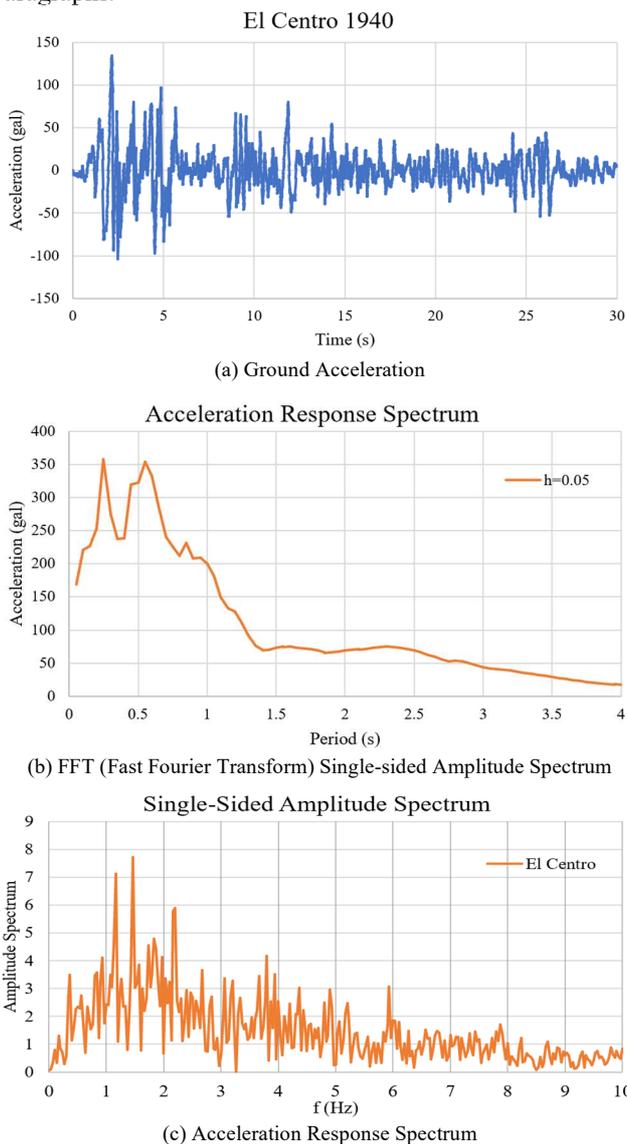

(c) Acceleration Response Spectrum

Fig. 21 El Centro Earthquake Input

A time history analysis was carried out to study the dynamic behavior of railway bridges under earthquake excitation. The first excitation is in the *Y* direction. Since the model is assumed to be in the elastic range, modal analysis with a 5% damping ratio was used to obtain the time history of members' responses (deformation and (absolute)

accelerations) in the *Y* direction. The acceleration time histories at the ground, at the upper frame, and the lower frame at the midspan are shown in Fig. 22(a).
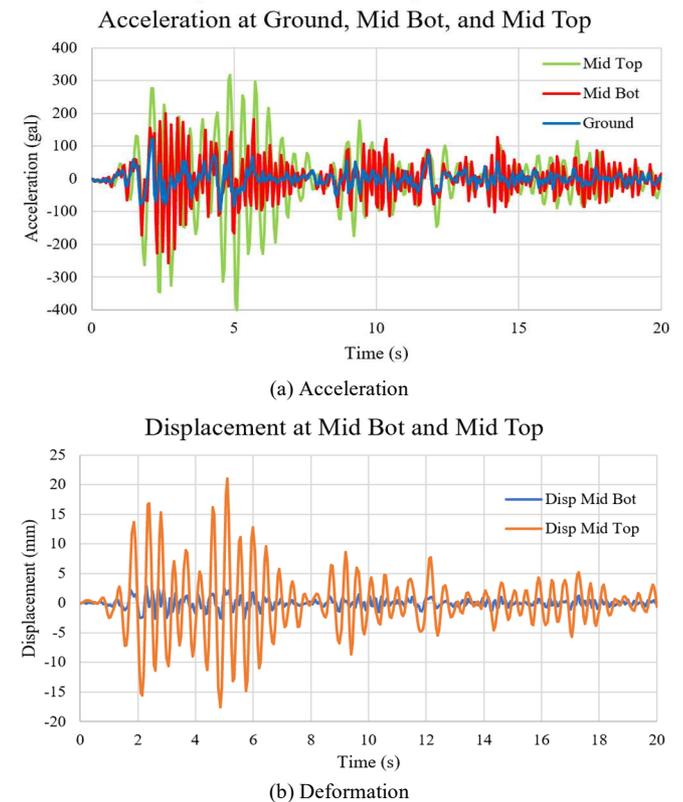

(a) Acceleration

(b) Deformation

Fig. 22 Time History of the Railway Bridge due to El Centro ground motion on Lateral (*Y*) Direction

As expected, the top frame's midspan acceleration is more significant than that of the bottom frame's midspan. The maximum acceleration at the upper frame reaches 399 gals at 5.1 seconds. The maximum acceleration at the lower frame reaches 256 gals at 2.7 seconds. Both peak accelerations take place at different times. This phenomenon is because the dominant frequency of the acceleration at the lower frame is higher (4.89 Hz) than at the upper frame (2.19 Hz).

These phenomena can be seen in Fig. 23(a) and 23(b). This result indicates that the lower frame member is stiffer than the upper frame in the lateral direction (*Y* direction). Fig. 22(b) illustrates deformation at the upper and lower frames at midspan in the *Y* direction. The deformation of the upper frame is much larger than that of the lower frame, as expected.

The second input acceleration is in the *Z* direction. For direct comparison, the input earthquake is applied for the discussed *Y* direction. The time history of accelerations at the upper frame and the lower frame at midspan are shown in Fig. 24(a). Both accelerations are almost similar and in agreement. Therefore, both of them are difficult to distinguish in the figure. The FFT of both accelerations shows identical results of dominant frequencies, that is, around 5.94 Hz, which is close to that of Modes 3 in Table 5. The results of numerical simulation for FFT acceleration are illustrated in Fig. 25. By applying a similar analysis for the recorded accelerations during and after the passing of trains over the railway bridge, the dynamic response of the bridge can be obtained. Decaying vibration is expected after the passing train, so the dynamic response with no train can also be observed.
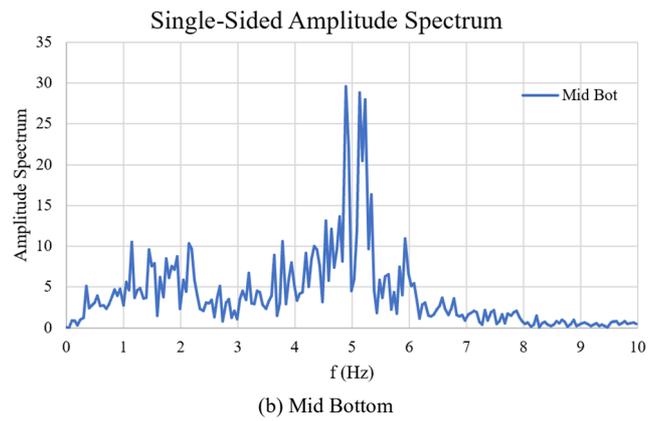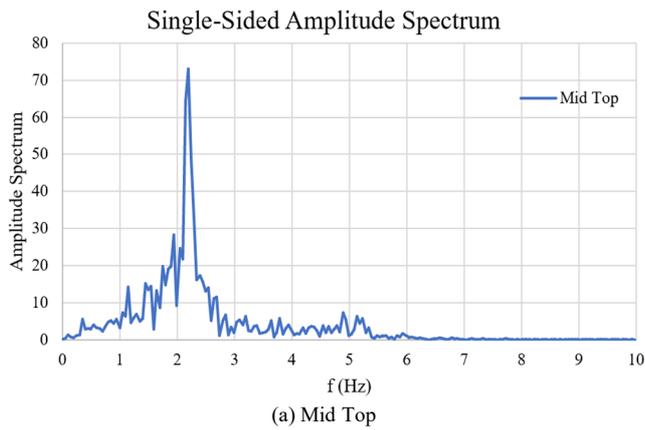
(a) Mid Top   (b) Mid Bottom

Fig. 23   Fast Fourier Transform (FFT) of Acceleration of the Railway Bridge due to El Centro ground motion on Lateral (Y) Direction

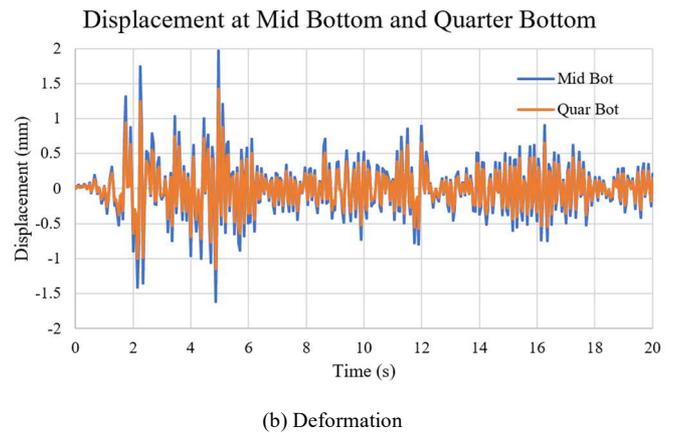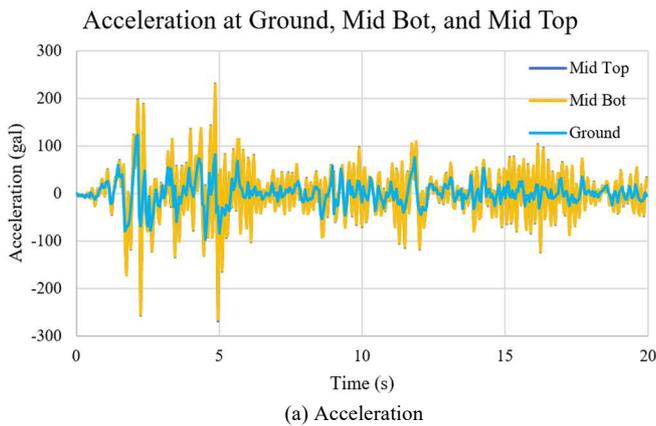

(a) Acceleration   (b) Deformation

Fig. 24   Time History of the Railway Bridge due to El Centro ground motion on Vertical (Z) Direction

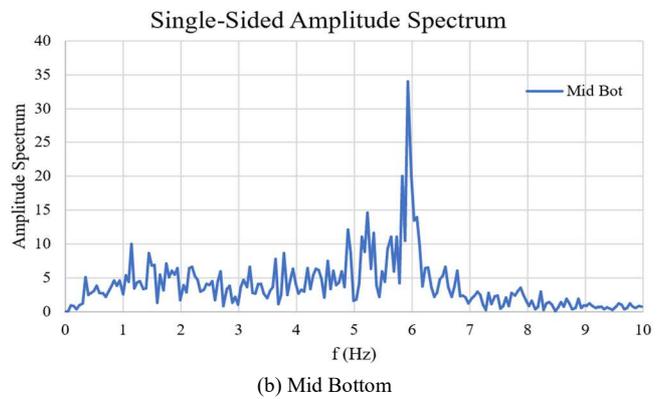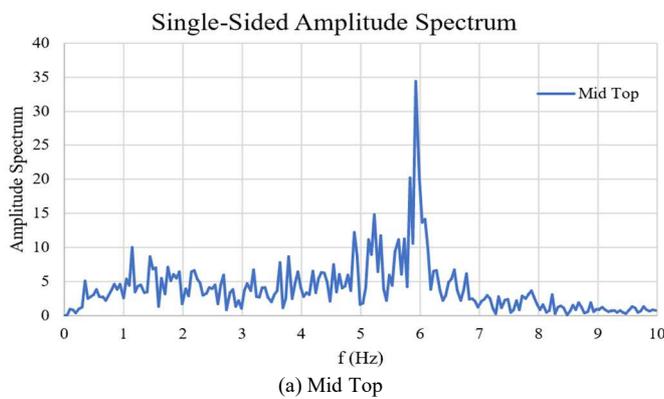(a) Mid Top   (b) Mid Bottom

Fig. 25   FFT of Acceleration of the Railway Bridge due to El Centro ground motion on Vertical (Z) Direction

IV. CONCLUSION

The direct analysis results of the steel railway bridge structure, field measurement, and numerical simulation facts are observed. The following concluding remarks are presented. This paper has discussed various aspects of the efforts to develop an SHM System for a steel railway bridge structure. As a result, the numerical analysis and field measurement show that the critical conditions are determined by deformation, while the stresses and natural frequencies are within safe boundary limits.

The loading effects on the existing railway bridge structures were effectively studied using finite element analysis in which a combination of load-carrying capacity and material properties were included. Characteristic values of the bridge loading conditions followed the applicable Indonesian National Standard. Conclusive results were found in determining the load-deformation characteristics of the railway bridge. The maximum deformation under dead load occurs in the middle of the railway bridge, measuring -7.65 mm in the Z direction. The maximum deformation generated by RM 1921 Load occurs at the midspan, measuring -50.58 mm in the Z direction. The maximum deformation caused by the dead load is much smaller (15%) than that due to RM 1921 load. The maximum deformation generated by a set of train loading occurs when the locomotive is at the midspan of the railway bridge, followed by

parts of a coach (Position II). The Position II train load gives the maximum deformation of -27.96 mm at Location 4. Nevertheless, the all-deformation values of the railway bridge are significantly less than those mentioned during the analysis.

The results of the numerical analysis and field measurement indicate that the axial force at the location of SG 03 (and 04) is the largest, measuring 599.00 kN. This axial force is caused by loading train Position II. As previously discussed, the moments at points of interest are relatively small, measuring 1.37 kN-m. Therefore, the stresses that are calculated from axial forces would be representative. The maximum stresses resulting from axial force occur at Position II of SG03, measuring 71.00 MPa. Train Position II produces the most significant stresses at all SG locations. The stress ratios at SG01, SG03, and SG05 locations are less than 35%. The stress ratios are still below the elastic limit. The stress ratio is the stress due to loads divided by the steel yield strength, which is 210 MPa.

Mode shapes and frequencies of the railway bridge model were observed when no train passed the railway bridge. The mode shape that will be excited by a passing train would be mode shape three because of its vertical movement. The mode shapes and natural frequencies calculated above are at the condition when the bridge is not passed by trains. The mode shape that will be excited by a passing train is expected to be Modes 3 or 4, as the movements are vertical. In summary, the results of this study indicate that the carrying capacity of railway bridges is relatively safe, provided regular maintenance and detailed monitoring are carried out.

AUTHORS' NOTE

The authors declare that they have no known competing financial interests or personal relationships that could have appeared to influence the work reported in this paper. The authors declare that there is no conflict of interest regarding the publication of this paper. The authors confirmed that the paper is free of plagiarism.

All authors of this manuscript are main contributors and have an equal primary role in conducting research according to their fields of expertise and publishing this article in highly reputable and globally indexed journals.

REFERENCES

[1] W. Barasa, T. Fiantika, D. A. Purnomo, and W. A. N. Aspar, "The comparative study of railway bridge design load between PM 60/2012 and EN 1991," *Maj. Ilm. Pengkaj. Ind.*, vol. 14, no. 2, pp. 107–116, Aug. 2020, doi: 10.29122/mipi.v14i2.4196.

[2] W. Barasa, W. A. N. Aspar, D. A. Purnomo, M. A. B. Nadi, T. Fiantika, and S. P. Primadiyanti, "Assessment of an existing steel railway bridge structure," *AIP Conf. Proceeding*, vol. 2689, Jul. 2023, doi: 10.1063/5.0115843.

[3] X. Sun, C. Guo, L. Yuan, Q. Kong, and Y. Ni, "Diffuse ultrasonic wave-based damage detection of railway tracks using PZT/FBG hybrid sensing system," *Sensors*, vol. 22, no. 7, p. 2504, Mar. 2022, doi: doi.org/10.3390/s22072504.

[4] M. R. Azim and M. Gül, "Damage detection framework for truss railway bridges utilizing statistical analysis of operational strain response," *Struct. Control Heal. Monit.*, vol. 27, no. 8, p. 34, 2020, doi:10.1002/stc.2573.

[5] J. Yang *et al.*, "A Review on damage monitoring and identification methods for arch bridges," *Buildings*, vol. 13, no. 8, p. 1975, 2023, doi:10.3390/buildings13081975.

[6] M. R. Azim, "A data-driven damage assessment tool for truss type railroad bridges using train induced strain time-history response," *Aust. J. Struct. Eng.*, vol. 22, no. 2, pp. 147–162, 2021, doi:10.1080/13287982.2021.1908710.

[7] A. Fernandez-Navamuel, D. Pardo, F. Magalhães, D. Zamora-Sánchez, Á. J. Omella, and D. Garcia-Sanchez, "Bridge damage identification under varying environmental and operational conditions combining Deep Learning and numerical simulations," *Mech. Syst. Signal Process. Syst. Signal Process.*, vol. 200, p. 110471, 2023, doi:10.1016/j.ymssp.2023.110471.

[8] X. Wang, Y. Zhuo, and S. Li, "Damage detection of high-speed railway box girder using train-induced dynamic responses," *Sustainability*, vol. 15, no. 11, p. 8852, 2023, doi:10.3390/su15118552.

[9] M. R. Azim and M. Gül, "Damage detection of steel-truss railway bridges using operational vibration data," *J. Struct. Eng.*, vol. 146, no. 3, Jan. 2020, doi: 10.1061/(ASCE)ST.1943-541X.0002547.

[10] M. J. Khosraviani, O. Baha, and S. H. Ghasemi, "Global and local damage detection in continuous bridge decks using instantaneous amplitude energy and cross-correlation function methods," *KSCE J. Civ. Eng.*, vol. 25, no. 2, pp. 603–620, 2021, doi: 10.1007/s12205-020-0622-0.

[11] Z. Li, Y. Lan, and W. Lin, "Investigation of frequency-domain dimension reduction for a2m-based bridge damage detection using accelerations of moving vehicles," *Materials (Basel).*, vol. 16, no. 5, p. 1872, Feb. 2023, doi: 10.3390/ma16051872.

[12] Y. B. Yang, Z.-L. Wang, K. Shi, H. Xu, and Y. T. Wu, "State-of-the-art of the vehicle-based methods for detecting the various properties of highway bridges and railway tracks," *Int. J. Struct. Stab. Dyn.*, vol. 20, no. 13, 2020, doi: 10.1142/S0219455420410047.

[13] A. Gomez-Cabrera and P. J. Escamilla-Ambrosio, "Review of machine-learning techniques applied to structural health monitoring systems for building and bridge structure," *Appl. Sci.*, vol. 12, no. 21, p. 10754, 2022, doi: 10.3390/app122110754.

[14] P. Russo and M. Schaerf, "Anomaly detection in railway bridges using imaging techniques," *Sci. Rep.*, vol. 13, p. 3916, 2023, doi:10.1038/s41598-023-30683-z.

[15] O. S. Sonbul and M. Rashid, "Algorithms and techniques for the structural health monitoring of bridges: Systematic literature review," *Sensors*, vol. 23, p. 4230, 2023, doi: 10.3390/s23094230.

[16] Z. Deng, M. Huang, N. Wan, and J. Zhang, "The current development of structural health monitoring for bridges: A review," *Buildings*, vol. 13, no. 6, p. 1360, 2023, doi: 10.3390/buildings13061360.

[17] K. Maes, L. Van Meerbeeck, E. P. B. Reynders, and G. Lombaert, "Validation of vibration-based structural health monitoring on retrofitted railway bridge KW51," *Mech. Syst. Signal Process.*, vol. 165, p. 108380, 2022, doi: 10.1016/j.ymssp.2021.108380.

[18] X. Li, Y. Xiao, H. Guo, and J. Zhang, "A BIM based approach for structural health monitoring of bridges," *KSCE J. Civ. Eng.*, vol. 26, no. 1, pp. 155–165, 2021, doi: 10.1007/s12205-021-2040-3.

[19] A. Pourtarki, H. B. Ghavifekr, and H. Afshin, "Study on the dynamic behaviour of Bafgh-Bandar Abbas Lane railway bridge for structural health monitoring purpose," *Aust. J. Struct. Eng.*, vol. 24, no. 3, pp. 243–253, 2023, doi: 10.1080/13287982.2022.2149975.

[20] S. S. Saidin, A. Jamadin, S. A. Kudus, N. M. Amin, and M. A. Anuar, "An overview: The application of vibration-based techniques in bridge structural health monitoring," *Int. J. Concr. Struct. Mater.*, vol. 16, no. 69, 2022, doi: 10.1186/s40069-022-00557-1.

[21] A. Meixedo, D. Ribeiro, J. Santos, R. Calçada, and M. Todd, "Progressive numerical model validation of a bowstring arch railway bridge based on a structural health monitoring system," *J. Civ. Struct. Heal. Monit.*, vol. 11, pp. 421–449, 2021, doi: 10.1007/s13349-020-00461-w.

[22] M. A. Mousa *et al.*, "Application of digital image correlation in structural health monitoring of bridge infrastructures: A review," *Infrastructures*, vol. 6, no. 176, 2021, doi: 10.3390/infrastructures6120176.

[23] Y. Fu, Y. Zhu, T. Hoang, K. Mechitov, and B. F. Spencer Jr., "xImpact: Intelligent wireless system for cost-effective rapid condition assessment of bridges under impacts," *Sensors*, vol. 22, no. 5701, 2022, doi: 10.3390/s22155701.

[24] F. Fu, T. Hoang, K. Mechitov, J. R. Kim, D. Zhang, and B. Spencer, "xShake: Intelligent wireless system for cost-effective real-time seismic monitoring of civil infrastructure," *Smart Struct. Syst.*, vol. 28, no. 4, pp. 483–497, 2021, doi: 10.12989/sss.2021.28.4.483.

[25] K. Zeng *et al.*, "Sensing mechanism and real-time bridge displacement monitoring for a laboratory truss bridge using hybrid data fusion," *Remote Sens.*, vol. 15, no. 3444, 2023, doi: 10.3390/rs15133444.

[26] R. Silva, D. Ribeirob, C. Costac, A. Arêdea, and R. Calçada, "Experimental validation of a non-linear train-track-bridge dynamic model of a stone arch railway bridge under freight traffic," *Int. J. Rail Transp.*, 2023, doi: 10.1080/23248378.2022.2133783.

[27] S. Chen, W. Kang, J. Yang, S. Dai, S. Zheng, and H. Jia, "Dynamic analysis of train–bridge coupling system for a long-span railway suspension bridge subjected to strike–slip fault," *Appl. Sci.*, vol. 13, no. 18, p. 10422, 2023, doi: 10.3390/app131810422.

[28] D. A. Purnomo, W. A. N. Aspar, W. Barasa, S. M. Harjono, P. Sukamdo, and T. Fiantika, "Initial implementation of structural health monitoring system of a railway bridge," *IOP Conf. Ser. Mater. Sci. Eng.*, vol. 1200, 2021, doi: 10.1088/1757-899X/1200/1/012019.

[29] P. Olaszek, I. Wyczałek, D. Sala, M. Kokot, and A. Swiercz, "Monitoring of the static and dynamic displacements of railway bridges with the use of inertial sensors," *Sensors*, vol. 20, no. 10, p. 2767, 2020, doi: 10.3390/s20102767.

[30] J. Lee, S. Jeong, J. Lee, S.-H. Sim, K.-C. Lee, and Y.-J. Lee, "Sensor data-based probabilistic monitoring of time-history deflections of railway bridges induced by high-speed trains," *Struct. Heal. Monit.*, vol. 21, no. 6, pp. 2518–2530, 2022, doi:10.1177/14759217211063424.

[31] Y. Ren, E. J. OBrien, D. Cantero, and J. Keenahan, "Railway bridge condition monitoring using numerically calculated responses from batches of trains," *Appl. Sci.*, vol. 12, p. 4972, 2022, doi: 10.3390/app12104972.

[32] P. König, P. Salcher, C. Adam, and B. Hirzinger, "Dynamic analysis of railway bridges exposed to high-speed trains considering the vehicle–track–bridge–soil interaction," *Acta Mech.*, vol. 232, pp. 4583–4608, 2021, doi: 10.1007/s00707-021-03079-1.

[33] D. Liu, B. Liu, X. Li, and K. Shi, "Theoretical and numerical examination of a novel method for identifying bridge moving force using an instrumented vehicle," *Buildings*, vol. 13, no. 6, p. 1481, 2023, doi: 10.3390/buildings13061481.

[34] W. Barasa *et al.*, "Monitoring displacement, strain, and acceleration of a steel railway bridge," *Ain Shams Eng. J.*, vol. 14, no. 11, 2023, doi:10.1016/j.asej.2023.102521.

[35] H. Kordestani, C. Zhang, and M. Shadabfar, "Beam damage detection under a moving load using random decrement technique and Savitzky–Golay Filter," *Sensors*, vol. 20, no. 1, p. 243, 2020, doi:10.3390/s20010243.

[36] Y. B. Yang, K. Shi, Z.-L. Wang, H. Xu, and Y. T. Wu, "Theoretical study on a dual-beam model for detection of track/bridge frequencies and track modulus by a moving vehicle," *Eng. Struct.*, vol. 244, p. 112726, 2021, doi: 10.1016/j.engstruct.2021.112726.

[37] M. Reiterer, L. Bettinelli, J. Schellander, A. Stollwitzer, and J. Fink, "Application of vehicle-based indirect structural health monitoring method to railway bridges—simulation and in situ test," *Appl. Sci.*, vol. 13, no. 19, p. 10928, 2023, doi:10.3390/app131910928.

[38] K. Chilamkuri and V. Kone, "Monitoring of varadhi road bridge using accelerometer sensor," *Mater. Today Proc.*, vol. 33, no. 1, pp. 367–371, 2020, doi: 10.1016/j.matpr.2020.04.159.

[39] T. Fiantika, W. A. N. Aspar, D. A. Purnomo, W. Barasa, S. M. Harjono, and S. P. Primadiyanti, "A review of structural health monitoring system and application for railway bridge," *AIP Conf. Proceeding*, vol. 2646, Apr. 2023, doi: 10.1063/5.0115843.

[40] M. R. Azim, H. Zhang, and M. Gül, "Damage detection of railway bridges using operational vibration data: theory and experimental verifications," *Struct. Monit. Maint.*, vol. 7, no. 2, pp. 149–166, Jun. 2020, doi: 10.12989/smm.2020.7.2.149.

[41] CSI 2016 Analysis Reference Manual for SAP2000, "Integrated finite elements analysis and design of structures tutorial manual." Computers and Struct. Inc. (CSI), Berkeley, CA, USA, [Online]. Available:

https://docs.csiamerica.com/manuals/sap2000/CSiRefer.pdf.

[42] D. De Domenico and E. Gandelli, "Advanced modeling of SMA flag-shaped hysteresis for nonlinear time-history analysis in SAP2000," *J. Struct. Eng.*, vol. 147, no. 11, 2002, doi:10.1061/(ASCE)ST.1943-541X.0003176.

[43] A. Tahmasebi and M. Rahimi, "Evaluation of nonlinear static and dynamic analysis of steel braced frame buildings subjected to near-field earthquakes using FBD and DBD," *Structures*, vol. 34, pp. 1364–1372, 2021, doi: 10.1016/j.istruc.2021.08.082.

[44] V. Shahsavari, M. Mehrkash, and E. Santini-Bell, "Damage detection and decreased load-carrying capacity assessment of a vertical-lift steel truss bridge," *J. Perform. Constr. Facil.*, vol. 34, no. 2, pp. 1–13, Apr. 2020, doi: 10.1061/ (ASCE)CF.1943-5509.0001400.

[45] SNI 1726-2019, *Indonesia National Standard: Seismic resistance of planning procedure for building and non-building structure.* Jakarta, Indonesia, 2019, p. 248 pp.

[46] Z.-W. Li, X.-Z. Liu, and S.-X. Chen, "A reliability assessment approach for slab track structure based on vehicle-track dynamics and surrogate model," *Proc. Inst. Mech. Eng. Part O J. Risk Reliab.*, vol. 236, no. 1, pp. 79–89, 2021, doi: 10.1177/1748006X211028405.

[47] D. M. Abdu, G. Wei, and W. Yang, "Assessment of railway bridge pier settlement based on train acceleration response using machine learning algorithms," *Structures*, vol. 5, pp. 598–608, 2023, doi: 10.1016/j.istruc.2023.03.167.

[48] R. Xi *et al.*, "Performance assessment of structural monitoring of a dedicated high-speed railway bridge using a moving-base RTK-GNSS method," *Remote Sens.*, vol. 15, no. 2, p. 3132, 2023, doi:10.3390/rs15123132.

[49] Z. He, W. Li, H. Salehi, H. Zhang, H. Zhou, and P. Jiao, "Integrated structural health monitoring in bridge engineering," *Autom. Constr.*, vol. 136, p. 104168, 2022, doi: 10.1016/j.autcon.2022.104168.

[50] J. Xin, Y. Jiang, J. Zhou, L. Peng, S. Liu, and Q. Tang, "Bridge deformation prediction based on SHM data using improved VMD and conditional KDE," *Eng. Struct.*, vol. 261, p. 114285, 2022, doi:10.1016/j.engstruct.2022.114285.

[51] S. Karimi and O. Mirza, "Damage identification in bridge structures: review of available methods and case studies," *Aust. J. Struct. Eng.*, vol. 24, no. 2, pp. 273–295, 2023, doi:10.1080/13287982.2022.2120239.

[52] M. R. Azim and M. Gül, "Development of a novel damage detection framework for truss railway bridges using operational acceleration and strain response," *Vibration*, vol. 4, no. 2, pp. 422–443, May 2021, doi:10.3390/vibration4020028.

[53] A. Malekjafarian, R. Corbally, and W. Gong, "A review of mobile sensing of bridges using moving vehicles: Progress to date, challenges and future trends," *Structures*, vol. 44, pp. 1466–1489, Oct. 2022, doi:10.1016/j.istruc.2022.08.075.

[54] D. Ribeiro, R. Calçada, M. Brehm, and V. Zabel, "Train–track–bridge dynamic interaction on a bowstring-arch railway bridge: Advanced modeling and experimental validation," *Sensors*, vol. 23, no. 1, p. 171, Jan. 2023, doi: 10.3390/s23010171.

[55] Y. Yu, L. Zhao, and C. Zhou, "A new vertical dynamic model for railway vehicle with passenger-train-track coupling vibration," *Proc. Inst. Mech. Eng. Part K J. Multi-body Dyn.*, vol. 234, no. 1, pp. 134–146, 2020, doi: 10.1177/1464419319879790.

[56] Transportation Minister of the Republic of Indonesia, *Regulation no. 60 of 2012: Railroad Technical Requirements.* Indonesia, 2012, p. 58 pp.

[57] PT. Kereta Api Indonesia (PT. KAI), "Specification for CC 206 Locomotive," Nov. 2015. https://id.wikipedia.org/wiki/Lokomotif_CC206 (accessed May 05, 2023).

[58] PT. INKA Indonesia, "Kereta Kelas Eksekutif Stainless Steel," 2017. https://www.inka.co.id/product/view/72 (accessed May 05, 2023).

[59] A. Meixedo, J. Santos, D. Ribeiro, R. Calçada, and M. Todd, "Damage detection in railway bridges using traffic-induced dynamic responses," *Eng. Struct.*, vol. 238, no. 112189, Mar. 2021, doi:10.1016/j.engstruct.2021.112189.

[60] F. P. Ulrich, "The Imperial valley earthquakes of 1940," *Bull. Seismol. Soc. Am.*, vol. 31, no. 1, pp. 13–31, Jan. 1941, doi:10.1785/BSSA0310010013.

[61] F. E. Udwadia and M. D. Trifunac, "Comparison of earthquake and microtremor ground motions in El Centro, California," *Bull. Seismol. Soc. Am.*, vol. 63, no. 4, pp. 1227–1253, Aug. 1973, doi:10.1785/BSSA0630041227.

[62] T. K. Rockwell and Y. Klinger, "Surface rupture and slip distribution of the 1940 Imperial Valley Earthquake, Imperial Fault, Southern California: Implications for rupture segmentation and dynamics," *Bull. Seismol. Soc. Am.*, vol. 103, no. 2A, pp. 629–640, Apr. 2013, doi:10.1785/0120120192.